ACS APPLIED MATERIALS & INTERFACES

Research Article

www.acsami.org

Two-Photon Sensing and Imaging of Endogenous Biological Cyanide in Plant Tissues Using Graphene Quantum Dot/Gold Nanoparticle Conjugate

Lili Wang,[†] Jing Zheng,[*,†] Sheng Yang,[‡] Cuichen Wu,[†] Changhui Liu,[†] Yue Xiao,[†] Yinhui Li,[†] Zhihe Qing,[‡] and Ronghua Yang[*,†,‡]

[†]State Key Laboratory of Chemo/Biosensing and Chemometrics, College of Chemistry and Chemical Engineering, Hunan University, Changsha 410082, China

[‡]School of Chemistry and Biological Engineering, Changsha University of Science and Technology, Changsha 410004, China

Supporting Information

ABSTRACT: One main source of cyanide (CN^-) exposure for mammals is through the plant consumption, and thus, sensitive and selective CN^- detection in plants tissue is a significant and urgent work. Although various fluorescence probes have been reported for CN^- in water and mammalian cells, the detection of endogenous biological CN^- in plant tissue remains to be explored due to the high background signal and large thickness of plant tissue that hamper the effective application of traditional one-photo excitation. To address these issues, we developed a new two-photo excitation (TPE) nanosensor using graphene quantum dots (GQDs)/gold nanoparticle (AuNPs) conjugate for sensing and imaging endogenous biological CN^-. With the benefit of the high quenching efficiency of AuNPs and excellent two-photon properties of GQDs, our sensing system can achieve a low detection limit of 0.52 μM and deeper penetration depth (about 400 μm) without interference from background signals of a complex biological environment, thus realizing sensing and imaging of CN^- in different types of plant tissues and even monitoring CN^- removal in food processing. To the best of our knowledge, this is the first time for fluorescent sensing and imaging of CN^- in plant tissues. Moreover, our design also provides a new model scheme for the development of two-photon fluorescent nanomaterial, which is expected to hold great potential for food processing and safety testing.

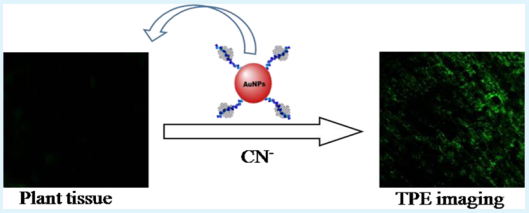

KEYWORDS: *cyanide, graphene quantum dot, gold nanoparticle, two-photon, plant tissue, imaging*

INTRODUCTION

Cyanide (CN^-), as a well-known anion present in plants and environment, is highly toxic to mammals and almost all other forms of life.[1−5] The toxicity of CN^- to mammals is mainly derived from its propensity to bind with the iron in cytochrome *c* oxidase, thus inducing the inhibition of mitochondrial electron chain transport and change of the cellular redox state,[6,7] etc. One main source of CN^- exposure for mammals is through the consumption of certain foods and plants. Therefore, it is significant to monitor CN^- in plants tissues.[8,9] Although many fluorescence probes have been reported so far for sensing and imaging of CN^- species in water and mammalian cells, the application in plant tissues remains to be explored.[10−13] As the traditional signal output method of fluorescence sensing technology, one-photon excitation (OPE) has its own limitations in complex environment, such as high background fluorescence and large photon loss owing to self-absorption and scattering, which thus restrict their monitoring of CN^- in plant tissues.[14,15]

Two-photon excitation (TPE) with near-infrared (NIR) photons as the excitation source is widely applied owing to its excellent advantages, such as lower tissue autofluorescence and self-absorption, lower photodamage and photobleaching, higher spatial resolution, and deeper penetration depth in biotissues.[16−19] To date, a variety of TPE fluorescence probes have been successfully developed for applications in chemical sensors and biological imagings.[20−22] Due to the extraordinary physical and chemical properties, graphene has sparked extensive applications in biosensing and bioimaging.[23−27] As a zero-dimensional graphene sheets, graphene quantum dots (GQDs) have attracted increasing attention in the field of biosensing and bioimaging owing to their special features, such as easy and cost-effective preparation, good biocompatibility, excellent photostability, and tunable fluorescence.[28−30] It is worth noting that the most important and attractive advantage of GQDs is their excellent two-photon property due to their large two-photon action cross sections, giving them huge potential for TPE signal output in complex biological environment.[31,32] Therefore, combining with the unique properties of TPE technique and GQDs, the development of GQD-based TPE nanosensor with lower biological autofluorescence and self-absorption, higher spatial resolution, and

Received: July 14, 2015
Accepted: August 12, 2015
Published: August 12, 2015

DOI: 10.1021/acsami.5b06352
ACS Appl. Mater. Interfaces 2015, 7, 19509−19515

deeper penetration depth has presented a promising potential in sensing and imaging of CN^- in plant tissues.

In this paper, we attempt to construct a peptide-mediated GQDs/gold nanoparticles (GQDs/AuNPs) hybrid nanosensor to achieve high performance of two-photon CN^- sensing and imaging in plant tissues. The AuNPs were functionalized with peptide molecules, the GQDs were assembled on the surface of AuNPs through $\pi-\pi$ stacking of GQDs and peptide to form the AuNP-PEP@GQDs nanosensor. In the absence of CN^-, the fluorescence of GQDs could be quenched by AuNPs through the fluorescence resonance energy transfer (FRET). Upon addition of CN^-, AuNPs would be etched, resulting in the disassembly of AuNP-PEP@GQDs. Consequently, the TPE fluorescence of GQDs could be restored effectively. Our results demonstrate that this AuNP-PEP@GQDs can serve as a sensitive fluorescent indicator for CN^- with a detection limit of 0.52 μM under optimal conditions. Compared with the separated dual-component system, the short distance between GQDs and AuNPs can result in the effective fluorescence quench of GQDs, thus realizing the sensitive detection of CN^-. Moreover, this assembled system is more stable when applied in a complex environment. More importantly, as it benefits from the two-photon properties of GQDs, this method can realize CN^- sensing and imaging in different types of plant tissues and further monitor its removal in the field of food processing. To the best of our knowledge, it is the first time CN^- fluorescent sensing and imaging has been applied in plant tissues. Furthermore, by changing the recognizing position, this method can be expanded to other biological relevant species sensing and imaging in vivo in future.

EXPERIMENTAL SECTION

Preparation of AuNP-PEP@GQDs Hybrid Nanosensor. Graphene oxide was synthesized from graphite powder according to Hummer's method.[33] The two-photon GQDs were synthesized following the method reported by Gong et al.[31] Citrate-stabilized AuNPs were prepared following Frens' method as reported previously.[34] All details were described in Supporting Information. The functionalization of AuNPs with the peptide was achieved by the Au−S chemistry. The peptide and AuNPs were mixed together at a fixed ratio at 4 °C for 24 h. Functionalized AuNPs were centrifuged at 12000 rpm for 15 min and washed three times with buffer. The number of peptides per AuNP was estimated by subtracting the amount of peptide in the supernatant from the total amount of peptide, which was added into the AuNPs solution. The concentration of peptide was calculated by UV−vis spectrum at 215 nm. The AuNP-PEP was redispersed in buffer, and GQDs with a final concentration of 5 μg/mL were then added. The solution was incubated at room temperature for 1 h to prepare AuNP-PEP@GQDs. Free GQDs were removed by centrifugation for 15 min at 12000 rpm followed by decantation of supernatants and redispersion in BR buffer (pH = 10). The final concentration of AuNP-PEP@GQDs was defined as the concentration of AuNPs and calculated using Lambert−Beer's law according to the following equation: $A = \varepsilon bc$, where the extinction coefficient (ε) is 2.78×10^8 $M^{-1}cm^{-1}$ for 13 nm AuNPs and b = 1.0 cm (for standard cuvettes).[35]

TPE Fluorescence Detection of CN^- in Vitro. To detect CN^- in vitro, we equilibrated aliquots (300 μL) of BR buffer containing 2 nM AuNP-PEP@GQDs and 100 μL solution containing different concentration of CN^- and reacted the solutions for 30 min. Then, the fluorescence of the above solutions was measured under two-photon excitation at 780 nm.

Preparation of the Plant Tissue Extract. Cassava, potato, sweet potato, and purple sweet potato were ground with a zest grater and subsequently homogenized with a pestle and mortar. The pretreatment process included soaking and washing. Cassava root was immersed in deionized water for 2 h; the deionized water was changed every 30 min, and then, the cassava root was washed three times. Different amounts of mashed plant tissues were diluted with 50 mL BR buffer and filtration. Aliquots of 100 μL of the supernatant were used for further analysis.

TPE Fluorescence Imaging of Plant Cells and Tissues. The cassava root was sliced into 0.2 mm thick. After 2 h, 100 μL AuNP-PEP@GQDs (2 nM) was distributed uniformly on the surface, and the two-photon imaging was carried out under an Olympus FV1000-MPE multiphoton laser scanning confocal microscope with a mode-locked titanium-sapphire laser source (120 fs pulse width, 80 MHz repetition rate) set at wavelength 780 nm (60× magnification). Slices of plant tissue 1 mm thick were freshly prepared. Afterward, 100 μL AuNP-PEP@GQDs (2 nM) was distributed uniformly on the surface. After 0.5 h, The two-photon imaging was carried out under an Olympus FV1000-MPE multiphoton laser scanning confocal microscope with a mode-locked titanium-sapphire laser source (120 fs pulse width, 80 MHz repetition rate) set at wavelength 780 nm. Z-scan imaging and the 3D two-photon confocal fluorescence images were collected along the Z-direction at depth of 0−600 μm (10 × magnification) of the plant tissue slice.

RESULTS AND DISCUSSION

Design Scheme. As shown in Scheme 1, the peptides (CGADDEFFFFDG) with cysteine residue are conjugated

Scheme 1. Schematic Illustration of AuNP-PEP@GQDs Nanosensor for CN^- Assay

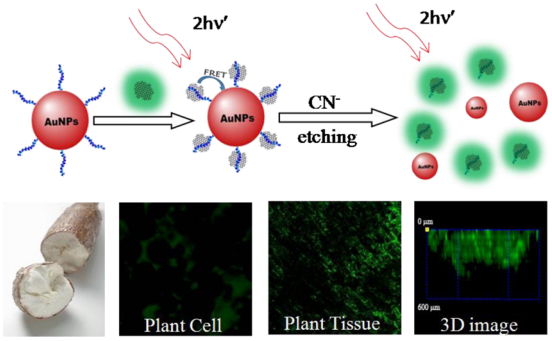

onto the surface of AuNPs through Au−S bond. The subsequent $\pi-\pi$ stacking interaction between peptide and GQDs can achieve successful assembly of AuNP-PEP@GQDs.[36] Before CN^- addition, AuNPs displayed extremely high quenching efficiency to GQDs due to the overlap between the emission spectrum of as-prepared GQDs and the absorption spectrum of AuNPs, which can satisfy the principle of FRET in our design.[37−40] In the presence of CN^-, AuNPs could be etched effectively and the disassembly of nanosensor can thus induce fluorescence recovery of GQDs.[41] After incubation with AuNP-PEP@GQDs, the CN^- released from plant tissue reacted with the hybrid nanosensor, resulting in obvious two-photon fluorescence signal recovery. Therefore, combined with the excellent properties of GQDs and TPE technology, the sensing and imaging of CN^- can be realized in plant tissues.

Fabrication and Characterization of the AuNP-PEP@GQDs Hybrid Nanosensor. Hybrid AuNP-PEP@GQDs nanosensor was synthesized via a multistep procedure, which involved synthesis of two-photon GQDs, AuNP-PEP conjugation, and final assembly of GQDs onto the surface of AuNPs. As a proof of concept, AuNPs were first prepared according to the reported method and transmission electron

DOI: 10.1021/acsami.5b06352
ACS Appl. Mater. Interfaces 2015, 7, 19509−19515

microscopy (TEM) image demonstrated a size distribution from 10 to 15 nm, most being 13 nm (Figure S1A). The maximum absorption of AuNPs was located at 518 nm (curve a, Figure S2). As an excellent two-photon nanomaterial, the GQDs were prepared through a facile one-pot solvothermal approach using graphene oxide as a precursor. TEM image (Figure S1B) showed the uniformly dispersed GQDs with an average diameter of 3.8 nm. High-resolution transmission electron microscopy (HRTEM) image depicted the clear graphene-like crystalline structure of GQDs, and the spacing of adjacent lattice planes was about 2.2 Å, which is close to the data of GQDs reported in reference and consistent with (002) diffraction plane of graphite (Inset of Figure S1B).[42] Then, UV−vis spectrum of GQDs in aqueous solution demonstrated an absorption band at 320 nm, which was similar to the reported GQDs (Figure S3).[31] The maximum emission wavelength of TPE located at 516 nm (curve b, Figure S2) which was also consistent with the previous reports.[31] The production yield of GQDs attained from GO is about 5.8%. Using rhodamine B (RhB) as a reference, the fluorescence quantum yield of GQDs in aqueous solution was measured to be 0.28 and the two-photon action cross section ($\delta \times \Phi$) was estimated to be 481 Goeppert−Mayer (GM) with excitation at 780 nm (curve a, Figure S4), which was obvious higher than the conventional organic dyes.[43] The two-photon absorption cross section (σ) based on the equation, $\sigma_b = \sigma_a \times (F_b/F_a) \times (\phi_b/\phi_a) \times (C_b/C_a)$, where F denotes the measured two-photon fluorescence intensity, ϕ stands for the one-photon quantum yield, and C is the concentration. The subscripts a and b represent the values for the GQDs and RhB, respectively.[44] Additionally, long-term stability of the two-photon dyes is crucial to their practical applications in biolabeling and bioimaging. Thus, the photostability of GQDs was also investigated through recording the fluorescence intensity with continuous UV-irradiation using Xe light (390 nm, 300 mW). After continuous UV-irradiation for 4 h, the fluorescence intensity of GQDs maintained constant while RhB demonstrated an obvious decrease (Figure S5). To demonstrate the capability of the as-prepared GQDs for two-photon imaging, we incubated GQDs with plant tissues, and the tissue became brightly illuminated with two-photon excitation at 780 nm after 2 h (Figure S6). Therefore, higher two-photon action cross section and good photostability have enabled GQDs become the effective fluorescence reporter for TPE sensing and imaging in complex biological samples.

After the successful synthesis of two nanoparticles, peptides were applied to link them together and construct a robust nanosensing conjugate for CN^- sensing. The peptide that contained cysteine residue was conjugated to AuNPs surface through thiol groups to form Au−S bonds and then absorbed GQDs through $\pi-\pi$ interaction, leading to shortened distance between the quencher and fluorophore. The UV−vis spectrum of AuNPs demonstrated about 3 nm red shift due to the increase of refractive index upon protein adsorption, confirming the successful conjugation of peptide (Figure S7).[45] Due to the overlap between two-photon emission wavelength of GQDs and absorption spectrum of AuNPs, the fluorescence intensity of GQDs in solution decreased upon the addition of AuNP-PEP and more than 87% quenching efficiency was achieved (Figure S8). In contrast, the quenching efficiency of GQDs was much weaker upon bare AuNPs addition (Figure S8 inset). The results demonstrated that the peptide could act as an effective linker to mediate assembly of AuNPs and GQDs, thus enhancing the quenching efficiency of AuNPs. The nanosensor was then further characterized by TEM, XPS and fluorescence anisotropy (FA). Representative TEM image showed that large AuNPs were surrounded by several small GQDs to form satellite structure (Figure 1A). The XPS survey spectrum of

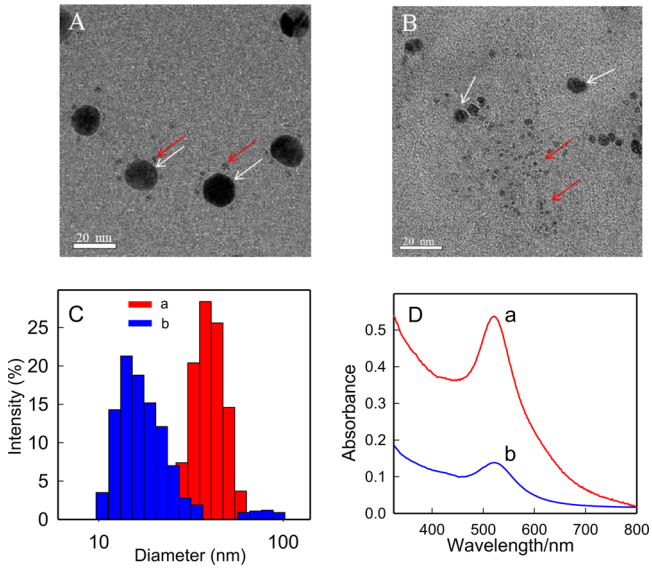

Figure 1. TEM images of 2 nM AuNP-PEP@GQDs before (A) and after (B) 500 μM CN^- addition. GQDs and AuNPs were indicated with red and white arrows, respectively. (C) DLS data and (D) UV−vis spectrum of 2 nM AuNP-PEP@GQDs (a) before and (b) after 500 μM CN^- addition.

AuNP-PEP@GQDs indicated three additional peaks at around 85.0, 334.0, and 353.0 eV, corresponding to the binding energies of Au 4f, Au $4d^5$, and Au $4d^3$, in contrast to GQDs (Figure S9). The FA value of free GQDs in buffer solution was very low while significant increase could be observed upon AuNP-PEP addition (Figure S10). These results clearly demonstrated that GQDs have been successfully assembled on the surface of AuNPs.

Validation of the Design Scheme. Before the CN^- detection, the effect of CN^- concentration to the fluorescence of GQDs was investigated, as shown in Figure S11. We could see that the fluorescence intensity is stable as a variation of CN^- concentration. To validate the scheme of AuNP-PEP@GQDs for CN^- detection, a series of experiments were further performed. First, the UV−vis spectral response of AuNPs upon CN^- addition was investigated and sharp absorbance decrease of AuNPs peaked at 518 nm could be observed (curve c, Figure S2). The result could confirm the etching effect of CN^- to AuNPs. Meanwhile, the color of solution containing AuNPs changed from red to colorless upon CN^- addition (Inset of Figure S2). Then, representative TEM image of AuNP-PEP@GQDs upon CN^- addition also displayed the etching of AuNPs since only a few small AuNPs and dispersed GQDs could be observed in Figure 1B. Dynamic light scattering (DLS) analysis also demonstrated the average hydrodynamic diameters of our constructed AuNP-PEP@GQDs decreased from 36.5 to 13.0 nm which was mainly due to the AuNPs etching (Figure 1C) and Zeta potential measurements revealed a remarkable charges elevation from −25.6 to −9.4 mV due to the disassembly of negatively charged AuNP-PEP@GQDs. Next, the typical UV−vis spectral response of AuNP-PEP@GQDs before and after

DOI: 10.1021/acsami.5b06352
ACS Appl. Mater. Interfaces 2015, 7, 19509−19515

incubation with CN^- was shown in Figure 1D. As expected, it was evident that a drastic absorption change could be observed, which further confirmed that AuNP-PEP@GQDs were etched upon CN^- addition. Additionally, the two-photon action cross section of AuNP-PEP@GQDs was estimated to be 52 GM while the value increased to 366 GM at 780 nm in the presence of CN^- (curves b and c, Figure S4) which is mainly due to the dissolution of AuNPs. Subsequently, we investigated the effect of CN^- to the fluorescence of AuNP-PEP@GQDs and typical OPE fluorescence response was demonstrated in Figure 2A.

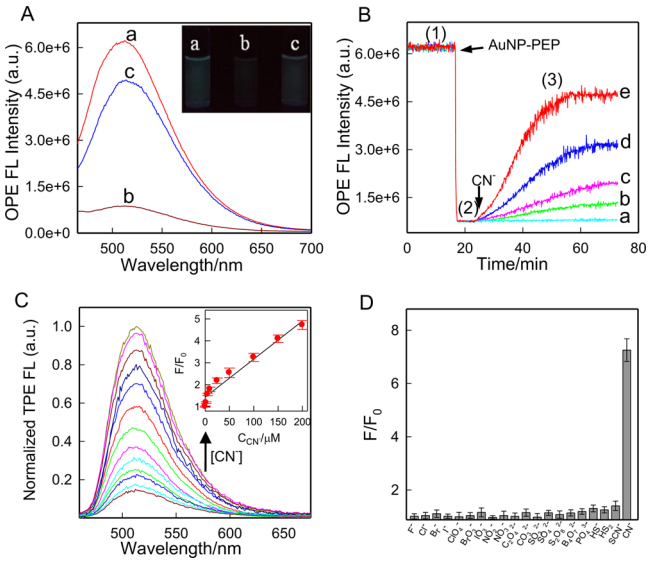

Figure 2. (A) Typical OPE fluorescence emission spectra of (a) 5 μg/mL GQDs, (b) upon addition of 2 nM AuNP-PEP, and (c) subsequently with 500 μM CN^- addition; (inset) photographs of the corresponding fluorescent species. (B) Real-time OPE fluorescence records of GQDs solution (5 μg/mL) upon addition of AuNP-PEP (2 nM), and subsequent addition of different concentrations of CN^- (a = 0 μM, b = 5 μM, c = 50 μM, d = 200 μM, e = 500 μM). For the measurement, we distinguished three steps: (1) the cuvette was filled with GQDs solution in BR buffer, (2) AuNP-PEP was added, and (3) CN^- was added. (C) Fluorescence spectra of AuNP-PEP@GQDs as functions of different concentrations of CN^- (0−500 μM) and (inset) TPE fluorescence intensity enhancement against CN^- concentration (0−200 μM), where F and F_0 are the fluorescence intensities of AuNP-PEP@GQDs in the presence or absence of CN^-. (D) Selectivity of AuNP-PEP@GQDs for CN^- over other anions at a concentration of 500 μM. The error bars signify the standard error obtained from three repetitive measurements.

Apparent fluorescence quenching occurred upon the addition of AuNP-PEP, and subsequent recovery could be observed after CN^- incubation. Finally, real-time dynamic OPE fluorescence intensity of GDQs was recorded as shown in Figure 2B. The results indicated that the fluorescence was almost completely quenched by AuNP-PEP, while the quenching was suppressed by the CN^- addition. The fluorescence recovery is proportionate to the concentration of CN^-, confirming the feasibility of our constructed nanosensor for CN^- detection.

Because the amount of peptide conjugated on AuNPs may influence the signal response of AuNP-PEP@GQDs to CN^-, the ratio of peptide to AuNPs was first optimized. The largest response was obtained with a loading capacity of about 40 peptide per AuNP (Figure S12). With increasing the amount of peptide, the F/F_0 value decreased, where F_0 and F represent the fluorescence intensity of AuNP-PEP@GQDs in the presence and absence of CN^-, attributing to the dense peptide can hinder the reaction between CN^- and AuNPs. In addition, the pH was also investigated in order to improve the sensitivity. As shown in Figure S13, the fluorescence recovery was tested under the pH range from 6.0 to 12.0. It was evident that this nanosensor exhibited the highest recovery efficiency at pH 10.0, which was chose in the subsequent experiments. The response at neutral condition is lower than basic condition also indicated that high pH value could decrease the competition for CN^- between the available protons and gold atoms.[46]

Under the optimized conditions, the response of this nanosensor to CN^- was carried out by TPE fluorescence spectrometry. Upon addition of CN^- (0−500 μM), a dose-dependent fluorescence recovery at 516 nm could be observed (Figure 2C). The intensity dynamically increased with the elevated CN^- concentration and a linear calibration graph was achieved within 1−200 μM (Figure 2C inset). The detection limit of 0.52 μM CN^- that was taken to be 3 times of the standard derivation in blank solution was achieved, which was than lower 1.9 μM, the maximum level of CN^- in drinking water permitted by the World Health Organization (WHO).[47] Compare with other reported CN^- sensing procedures, the sensitivity of the present system is comparable (Table S1). To evaluate the selectivity of this nanosensor, we also investigated the influence of other common anions. As shown in Figure 2D, all of these tested anions, including SCN^-, H_2S, HS^-, $B_4O_7^{2-}$, Br^-, BrO_3^-, Cl^-, ClO_4^-, CO_3^{2-}, $C_2O_4^{2-}$, F^-, I^-, IO^{3-}, NO^{2-}, NO^{3-}, PO_4^{3-}, SO_3^{2-}, SO_4^{2-}, and $S_2O_8^{2-}$, did not show obvious response. However, only the presence of CN^- could present a remarkable turn-on response. This excellent selectivity can be attributed to the unique Elsner reaction between CN^- and Au atoms.[48]

AuNP-PEP@GQDs Hybrid Nanosensor for CN^- Detection in Plant Tissue Extract by OPE and TPE Technique. After demonstrating in vitro sensing of CN^- by AuNP-PEP@GQDs, we next explored its potential in quantification of CN^- in plant tissues. Because the roots of cassava are a well-known source of endogenous biological CN^-, it was chosen as the model plant tissue for CN^- measurement. The aqueous extracts of these roots were prepared according to the reported procedure.[49] As shown in Figure 3A, the OPE emission spectra of cassava extract revealed a high autofluorescence signal which overlapped with the emission of GQDs. The high background signal of cassava extract would impede the sensitive detection of CN^-. In contrast, the background fluorescence of cassava extract was much weaker under TPE method while a remarkable enhancement was achieved upon CN^- addition (Figure 3B). For the quantitative assessment of CN^- in cassava, the extracts were first prepared from varied amounts of cassava. Then, an aliquot of the as-constructed AuNP-PEP@GQDs suspension was incubated with cassava extract. The fluorescence was measured under TPE fluorescence spectroscopy and a linear response as the amount of cassava increased could be observed (from 0 to 20 g, curve a, Figure 3C). It is worth noting that the response was less sensitive under OPE method than using TPE hough the fluorescence recovery of GQDs, which is mainly because of the high background fluorescence under OPE (curve b, Figure 3C). We then quantified the amount of CN^- in cassava root using a standard addition approach. The amount of CN^- in cassava was estimated to be (9.4 ± 0.5) mg per 100 g of cassava, which was in a good agreement with the normal range of CN^- content.[50] For the other plant tissues, the extract of commercially available potato,

DOI: 10.1021/acsami.5b06352
ACS Appl. Mater. Interfaces 2015, 7, 19509−19515

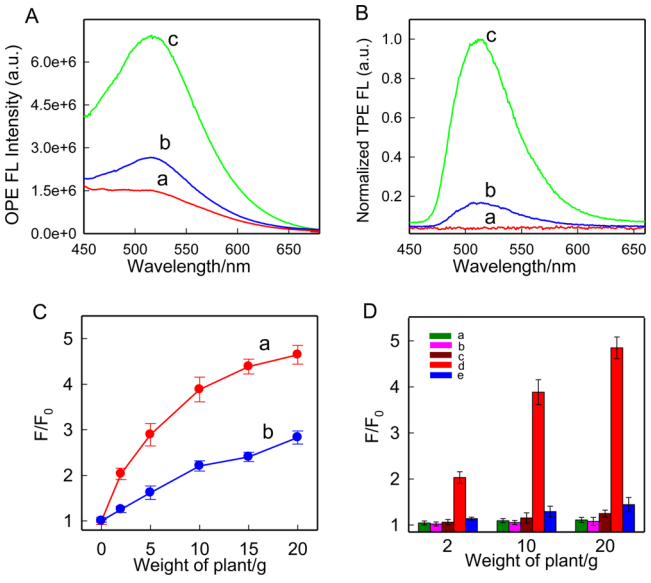

Figure 3. (A) OPE and (B) TPE spectra of (a) the cassava extract, (b) AuNP-PEP@GQDs (2 nM) in pretreated cassava extract, and (c) AuNP-PEP@GQDs in pretreated cassava extract upon 500 μM CN^- addition. (C, a) TPE and (d) OPE fluorescence enhancement (F/F_0) of AuNP-PEP@GQDs at 516 nm as functions of the increasing amount of cassava, where F and F_0 are the fluorescence intensity of AuNP-PEP@GQDs in the absence or presence of cassava extract. (D) TPE fluorescence enhancement (F/F_0) of the AuNP-PEP@GQDs as functions of different amount of plant tissue extract from (a) potato, (b) sweet potato, (c) purple sweet potato, and (d) cassava before (e) and after soaking and washing. The error bars signify the standard error obtained from three repetitive measurements.

sweet potato and purple sweet potato were also tested for their CN^- content. However, after incubation with potato, sweet potato, and purple sweet potato extract, no significant fluorescence emission signal changes of AuNP-PEP@GQDs could be observed (column a-c, Figure 3D). This TPE method was further used to monitor the removing effect of cassava pretreatment. Fresh cassava extract demonstrated an elevated fluorescence recovery which was dependent on the amount of cassava (column d, Figure 3D). However, after the cassava root was soaked for 2 h and washed three times, the extract demonstrate negligible fluorescence increments even at higher concentration (column e, Figure 3D). Therefore, these results demonstrated that our strategy could be used for the quantitative detection of endogenous CN^- in different plant tissues and also indicated, the pretreatment such as soaking and washing could remove the endogenous CN^- in plant tissues efficiently.

AuNP-PEP@GQDs Hybrid Nanosensor for CN^- Imaging in Plant Tissues. After the response of the CN^- sensor was achieved in vitro, TPE confocal fluorescence imaging was performed to demonstrate the applicability of endogenous CN^- imaging in plant cells and tissues. The fresh cassava was sliced into 0.2 mm thick pieces and incubated with AuNP-PEP@GQDs. Thus, the cassava cells could be clearly observed with a diameter of ~12 μm. When the cassava tissues are damaged, the linamarase contact with cyanogenic glycosides, which results in its hydrolysis and thus leads to the release of CN^-.[49] Based on this, an intense TPE fluorescence signal could be observed, as shown in Figure 4A. On the contrary, negligible fluorescence could be observed after soaking and washing (Figure 4B), indicating the removal of CN^- after pretreatment.

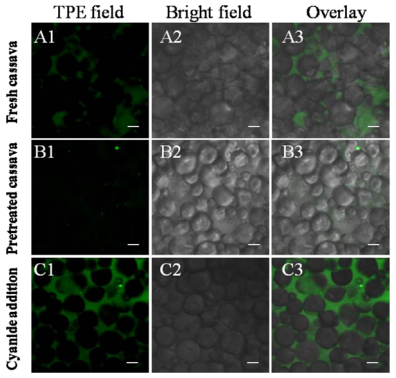

Figure 4. TPE images of (A) the fresh cassava cell, (B) cassava cell pretreated by soaking and washing, and (C) 200 μM CN^- preincubated cassava cell after incubation with AuNP-PEP@GQDs (2 nM) for 2 h. Scale bar: 10 μm.

Meanwhile, the green fluorescence was much brighter and widespread after preincubated with CN^- (Figure 4C). All these results can demonstrate that AuNP-PEP@GQDs could be used for sensing CN^- distribution and removal in cassava cells.

The course of the enzymatic liberation of CN^- from plant tissue was followed by TPE imaging directly on the surface of freshly cut slices. The fresh cassava and potato slices were stored at room temperature for different times and then incubated with AuNP-PEP@GQDs. The overall TPE fluorescence intensity of cassava increased as the function of time and reached maximum after 1.5 h (Figure 5A). In contrast, the TPE fluorescence of potato slices was constantly weak, even with increased the incubation time (Figure 5B). For sweet potato and purple sweet potato, the fluorescence signal of two slices were also negligible after incubated with AuNP-PEP@GQDs (Figure S14). More importantly, the fresh cassava slice

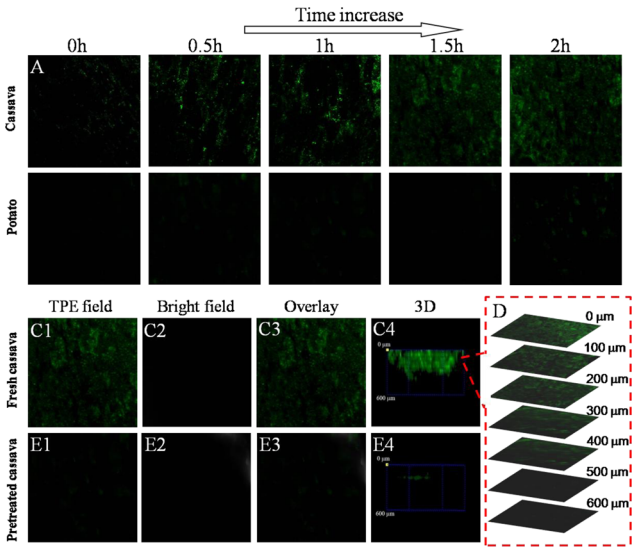

Figure 5. TPE imaging of (A) fresh cassava slice and (B) potato slice after incubated with 100 μL AuNP-PEP@GQDs (2 nM) with an increase of incubation time. TPE images of (C) fresh cassava slice and (E) pretreated cassava slice after incubated with 100 μL AuNP-PEP@GQDs for 2 h. (D) Confocal Z-scan TPE sections of the nanosensor incubated cassava slice at different penetration depths. Scale bar: 100 μm. The corresponding 3D images are accumulated along the Z-direction at depths of 0−600 μm.

DOI: 10.1021/acsami.5b06352
ACS Appl. Mater. Interfaces 2015, 7, 19509−19515

incubated with AuNP-PEP@GQDs demonstrated distinct TPE fluorescence at a depth of 100 μm (Figure 5C). The Z-scanning confocal imaging showed that TPE fluorescence can still be clearly sensed up to 400 μm of penetration depth (Figure 5D), which was much deeper than that obtained from OPE imaging (Figure S15). All these results demonstrated that CN^- existed in cassava, and liberation can be completed within 1.5 h. In contrast, no significant endogenous CN^- was present in sweet potato and purple sweet potato, which further confirmed that our constructed AuNP-PEP@GQDs nanosensor could be used for sensing and imaging of CN^- directly in plant tissue.

Enzymatic release of CN^- in cassava, which is the third most important food source in the tropical world, can cause disastrous consequences.[51] Thus, adequate cassava removal processing is of importance in eliminating the toxic cassava and converting them into safe food.[52] To remove CN^-, a pretreatment strategy was employed, and the corresponding CN^- release from cassava sample was monitored by TPE imaging. After soaking for 2 h and being wash three times with buffer solution, the removal efficiency of CN^- in cassava was investigated. Only negligible fluorescence was observed after AuNP-PEP@GQDs were poured and incubated on pretreated cassava slices, as shown in Figure 5E, which further indicated that CN^- has been removed efficiently after pretreatment. On the contrary, when the cassava slices were preincubated with CN^-, stronger green fluorescence was observed (Figure S16). These results demonstrated that our constructed nanosensor can be used for high-contrast TPE imaging of CN^- in deep plant tissue and applied for the direct monitoring of CN^- removal during food processing in future.

CONCLUSION

In summary, we proposed a highly sensitive nanosensor based on GQDs for TPE sensing and imaging of CN^- in plant tissues. Through the destruction of FRET process from GQDs to AuNPs, this AuNP-PEP@GQDs nanosensor could be used as an effective probe for highly selective detection of CN^- in vitro with a detection limit of 0.52 μM under optimal condition could be achieved. Combing with the excellent two-photon properties of GQDs, this sensor could be employed to reduce the high background signal of complex biological environment and thus realize sensing and imaging of CN^- in different types of plant tissues, even monitoring CN^- removal in food processing. To the best of our knowledge, this is the first time fluorescent sensing and imaging of CN^- in plant tissues have been applied, which will offer a new approach for monitoring the CN^- removal. Moreover, benefited from the unique properties of nanostructured materials and the TPE technique, this new AuNP-PEP@GQDs-based strategy for developing robust biomolecules sensors is expected to hold great potential for food processing and safety testing.

ASSOCIATED CONTENT

Supporting Information

The Supporting Information is available free of charge on the ACS Publications website at DOI: 10.1021/acsami.5b06352.

More details about chemicals and reagents, synthesis and characterizations of GQDs and AuNPs, and spectroscopic data as noted in text. (PDF)

AUTHOR INFORMATION

Corresponding Authors

*E-mail: zhengjing2013@hnu.edu.cn.

*E-mail: Yangrh@pku.edu.cn. Fax: +86-731-88822523.

Notes

The authors declare no competing financial interest.

ACKNOWLEDGMENTS

We are grateful for the financial support through the National Natural Science Foundation of China (21405038, 21135001 and 21305036), the Foundation for Innovative Research Groups of NSFC (21221003), the "973" National Key Basic Research Program (2011CB91100-0), and the Fundamental Research Funds for the Central Universities.

REFERENCES

(1) Panda, M.; Robinson, N. C. Kinetics and Mechanism for the Binding of HCN to Cytochrome C Oxidase. *Biochemistry* **1995**, *34*, 10009−10018.

(2) Koenig, R. Wildlife Deaths Are a Grim Wake-Up Call in Eastern Europe. *Science* **2000**, *287*, 1737−1738.

(3) Wang, F.; Wang, L.; Chen, X. Q.; Yoon, J. Y. Recent Progress in the Development of Fluorometric and Colorimetric Chemosensors for Detection of Cyanide Ions. *Chem. Soc. Rev.* **2014**, *43*, 4312−4324.

(4) Conn, E. E. Cyanogenic Glycosides. *J. Agric. Food Chem.* **1969**, *17*, 519−526.

(5) Poulton, J. E. Cyanogenesis in Plants. *Plant Physiol.* **1990**, *94*, 401−405.

(6) Badugu, R.; Lakowicz, J. R.; Geddes, C. D. Enhanced Fluorescence Cyanide Detection at Physiologically Lethal Levels: Reduced ICT-Based Signal Transduction. *J. Am. Chem. Soc.* **2005**, *127*, 3635−3641.

(7) Oluwole, O. S. A.; Onabolu, A. O.; Mtunda, K.; Mlingi, N. Characterization of Cassava (Manihot esculenta Crantz) Varieties in Nigeria and Tanzania, and Farmers' Perception of Toxicity of Cassava. *J. Food Compos. Anal.* **2007**, *20*, 559−567.

(8) Zelder, F.; Tivana, L. Corrin-based Chemosensors for the ASSURED Detection of Endogenous Cyanide. *Org. Biomol. Chem.* **2015**, *13*, 14−17.

(9) Kaur, K.; Saini, R.; Kumar, A.; Luxami, V.; Kaur, N.; Singh, P.; Kumar, S. Chemodosimeters: An Approach for Detection and Estimation of Biologically and Medically Relevant Metal Ions, Anions and Thiols. *Coord. Chem. Rev.* **2012**, *256*, 1992−2028.

(10) Liu, J. L.; Liu, Y.; Liu, Q.; Li, C. Y.; Sun, L. N.; Li, F. Y. Iridium(III) Complex-Coated Nanosystem for Ratiometric Upconversion Luminescence Bioimaging of Cyanide Anions. *J. Am. Chem. Soc.* **2011**, *133*, 15276−15279.

(11) Cheng, X. H.; Tang, R. L.; Jia, H. Z.; Feng, J.; Qin, J. G.; Li, Z. New Fluorescent and Colorimetric Probe for Cyanide: Direct Reactivity, High Selectivity, and Bioimaging Application. *ACS Appl. Mater. Interfaces* **2012**, *4*, 4387−4392.

(12) Zong, C. H.; Zheng, L. R.; He, W. H.; Ren, X. Y.; Jiang, C. H.; Lu, L. H. In Situ Formation of Phosphorescent Molecular Gold(I) Cluster in a Macroporous Polymer Film to Achieve Colorimetric Cyanide Sensing. *Anal. Chem.* **2014**, *86*, 1687−1692.

(13) Yuan, L.; Lin, W. Y.; Yang, Y. T.; Song, J. Z.; Wang, J. L. Rational Design of a Highly Reactive Ratiometric Fluorescent Probe for Cyanide. *Org. Lett.* **2011**, *13*, 3730−3733.

(14) Yi, M.; Yang, S.; Peng, Z. Y.; Liu, C. H.; Li, J. S.; Zhong, W. W.; Yang, R. H.; Tan, W. H. Two-Photon Graphene Oxide/Aptamer Nanosensing Conjugate for In Vitro or In Vivo Molecular Probing. *Anal. Chem.* **2014**, *86*, 3548−3554.

(15) Yan, H. J.; He, L. L.; Zhao, W. J.; Li, J. S.; Xiao, Y.; Yang, R. H.; Tan, W. H. Poly β-Cyclodextrin/TPdye Nanomicelle-based Two-Photon Nanoprobe for Caspase-3 Activation Imaging in Live Cells and Tissues. *Anal. Chem.* **2014**, *86*, 11440−11450.

(16) Parthenopoulos, D. A.; Rentzepis, P. M. Three-Dimensional Optical Storage Memory. *Science* **1989**, *245*, 843−845.
(17) Helmchen, F.; Denk, W. Deep Tissue Two-photon Microscopy. *Nat. Methods* **2005**, *2*, 932−940.
(18) Kim, H. M.; Cho, B. R. Two-Photon Probes for Intracellular Free Metal Ions, Acidic Vesicles, And Lipid Rafts in Live Tissues. *Acc. Chem. Res.* **2009**, *42*, 863−872.
(19) Bae, S. K.; Heo, C. H.; Choi, D. J.; Sen, D.; Joe, E. H.; Cho, B. R.; Kim, H. M. A Ratiometric Two-Photon Fluorescent Probe Reveals Reduction in Mitochondrial H_2S Production in Parkinson's Disease Gene Knockout Astrocytes. *J. Am. Chem. Soc.* **2013**, *135*, 9915−9923.
(20) Zhang, W.; Li, P.; Yang, F.; Hu, X. F.; Sun, C. Z.; Zhang, W.; Chen, D. Z.; Tang, B. Dynamic and Reversible Fluorescence Imaging of Superoxide Anion Fluctuations in Live Cells and in Vivo. *J. Am. Chem. Soc.* **2013**, *135*, 14956−14959.
(21) Kang, D. E.; Lim, C. S.; Kim, J. Y.; Kim, E. S.; Chun, H. J.; Cho, B. R. Two-Photon Probe for Cu^{2+} with an Internal Reference: Quantitative Estimation of Cu^{2+} in Human Tissues by Two-Photon Microscopy. *Anal. Chem.* **2014**, *86*, 5353−5359.
(22) Lee, H. Y.; Heo, C. H.; Sen, D.; Byun, H.; Kwak, I. H.; Yoon, G.; Kim, H. M. Ratiometric Two-Photon Fluorescent Probe for Quantitative Detection of β-Galactosidase Activity in Senescent Cells. *Anal. Chem.* **2014**, *86*, 10001−10005.
(23) Wang, Y.; Tang, L. H.; Li, Z. H.; Lin, Y. H.; Li, J. H. In Situ Simultaneous Monitoring of ATP and GTP Using a Graphene Oxide Nanosheet-based Sensing Platform in Living Cells. *Nat. Protoc.* **2014**, *9*, 1944−1955.
(24) Lu, C. H.; Yang, H. H.; Zhu, C. L.; Chen, X.; Chen, G. N. A Graphene Platform for Sensing Biomolecules. *Angew. Chem., Int. Ed.* **2009**, *48*, 4785−4787.
(25) Yin, P. T.; Shah, S.; Chhowalla, M.; Lee, K. B. Design, Synthesis, and Characterization of Graphene-Nanoparticle Hybrid Materials for Bioapplications. *Chem. Rev.* **2015**, *115*, 2483−2531.
(26) Wang, Y.; Li, Z. H.; Li, J. H.; Lin, Y. H. Graphene and Graphene Oxide: Biofunctionalization and Applications in Biotechnology. *Trends Biotechnol.* **2011**, *29*, 205−212.
(27) Lin, L.; Liu, Y.; Zhao, X.; Li, J. H. Sensitive and Rapid Screening of T4 Polynucleotide Kinase Activity and Inhibition based on Coupled Exonuclease Reaction and Graphene Oxide Platform. *Anal. Chem.* **2011**, *83*, 8396−8402.
(28) Tetsuka, H.; Asahi, R.; Nagoya, A.; Okamoto, K.; Tajima, I.; Ohta, R.; Okamoto, A. Optically Tunable Amino-Functionalized Graphene Quantum Dots. *Adv. Mater.* **2012**, *24*, 5333−5338.
(29) Nurunnabi, M.; Khatun, Z.; Huh, K. M.; Park, S. Y.; Lee, D. Y.; Cho, K. J.; Lee, Y. K. In Vivo Biodistribution and Toxicology of Carboxylated Graphene Quantum Dots. *ACS Nano* **2013**, *7*, 6858−6867.
(30) Yang, S. W.; Sun, J.; He, P.; Deng, X. X.; Wang, Z. Y.; Hu, C. Y.; Ding, G. Q.; Xie, X. M. Selenium Doped Graphene Quantum Dots as an Ultrasensitive Redox Fluorescent Switch. *Chem. Mater.* **2015**, *27*, 2004−2011.
(31) Liu, Q.; Guo, B. D.; Rao, Z. Y.; Zhang, B. H.; Gong, J. R. Strong Two-Photon-Induced Fluorescence from Photostable, Biocompatible Nitrogen-Doped Graphene Quantum Dots for Cellular and Deep-Tissue Imaging. *Nano Lett.* **2013**, *13*, 2436−2441.
(32) Zhu, A. W.; Ding, C. Q.; Tian, Y. A Two-photon Ratiometric Fluorescence Probe for Cupric Ions in Live Cells and Tissues. *Sci. Rep.* **2013**, *3*, 2933.
(33) Hummers, W. S.; Offeman, R. E. Preparation of Graphitic Oxide. *J. Am. Chem. Soc.* **1958**, *80*, 1339−1339.
(34) Frens, G. Controlled Nucleation for the Regulation of the Particle Size in Monodisperse Gold Suspensions. *Nature, Phys. Sci.* **1973**, *241*, 20−22.
(35) Yguerabide, J.; Yguerabide, E. E. Light-Scattering Submicroscopic Particles as Highly Fluorescent Analogs and Their Use as Tracer Labels in Clinical and Biological Applications: I. Theory. *Anal. Biochem.* **1998**, *262*, 137−156.
(36) Feng, B. Y.; Guo, L. J.; Wang, L. H.; Li, F.; Lu, J. X.; Gao, J. M.; Fan, C. H.; Huang, Q. A Graphene Oxide-Based Fluorescent Biosensor for the Analysis of Peptide−Receptor Interactions and Imaging in Somatostatin Receptor Subtype 2 Overexpressed Tumor Cells. *Anal. Chem.* **2013**, *85*, 7732−7737.
(37) Fan, C. H.; Wang, S.; Hong, J. W.; Bazan, G. C.; Plaxco, K. W.; Heeger, A. J. Beyond Superquenching: Hyper-efficient Energy Transfer from Conjugated Polymers to Gold Nanoparticles. *Proc. Natl. Acad. Sci. U. S. A.* **2003**, *100*, 6297−6301.
(38) Oh, E.; Hong, M. Y.; Lee, D.; Nam, S. H.; Yoon, H. C.; Kim, H. S. Inhibition Assay of Biomolecules based on Fluorescence Resonance Energy Transfer (FRET) between Quantum Dots and Gold Nanoparticles. *J. Am. Chem. Soc.* **2005**, *127*, 3270−3271.
(39) Wu, P. G.; Brand, L. Resonance Energy Transfer: Methods and Applications. *Anal. Biochem.* **1994**, *218*, 1−13.
(40) Clegg, R. M. Fluorescence Resonance Energy Transfer. *Curr. Opin. Biotechnol.* **1995**, *6*, 103−110.
(41) McCarthy, A. J.; Coleman, R. G.; Nicol, M. J. The Mechanism of the Oxidative Dissolution of Colloidal Gold in Cyanide Media. *J. Electrochem. Soc.* **1998**, *145*, 408−414.
(42) Sun, H. J.; Gao, N.; Wu, L.; Ren, J. S.; Wei, W. L.; Qu, X. G. Highly Photoluminescent Amino-Functionalized Graphene Quantum Dots Used for Sensing Copper Ions. *Chem. - Eur. J.* **2013**, *19*, 13362−13368.
(43) Zhou, L. Y.; Zhang, X. B.; Wang, Q. Q.; Lv, Y. F.; Mao, G. J.; Luo, A. L.; Wu, Y. X.; Wu, Y.; Zhang, J.; Tan, W. H. Molecular Engineering of a TBET-Based Two-Photon Fluorescent Probe for Ratiometric Imaging of Living Cells and Tissues. *J. Am. Chem. Soc.* **2014**, *136*, 9838−9841.
(44) Xu, C.; Webb, W. W. Measurement of Two-photon Excitation Cross Sections of Molecular Fluorophores with Data from 690 to 1050 nm. *J. Opt. Soc. Am. B* **1996**, *13*, 481−491.
(45) Liu, X. H.; Wang, Y.; Chen, P.; Wang, Y. S.; Zhang, J. L.; Aili, D.; Liedberg, B. Biofunctionalized Gold Nanoparticles for Colorimetric Sensing of Botulinum Neurotoxin A Light Chain. *Anal. Chem.* **2014**, *86*, 2345−2352.
(46) Liu, Y. L.; Ai, K. L.; Cheng, X. L.; Huo, L. H.; Lu, L. H. Gold-Nanocluster-Based Fluorescent Sensors for Highly Sensitive and Selective Detection of Cyanide in Water. *Adv. Funct. Mater.* **2010**, *20*, 951−956.
(47) Dai, Z.; Boon, E. M. Engineering of the Heme Pocket of an H-NOX Domain for Direct Cyanide Detection and Quantification. *J. Am. Chem. Soc.* **2010**, *132*, 11496−11503.
(48) Wang, X. B.; Wang, Y. L.; Yang, J.; Xing, X. P.; Li, J.; Wang, L. S. Evidence of Significant Covalent Bonding in $Au(CN)_2^-$. *J. Am. Chem. Soc.* **2009**, *131*, 16368−16370.
(49) Mannel-Croise, C.; Probst, B.; Zelder, F. A Straightforward Method for the Colorimetric Detection of Endogenous Biological Cyanide. *Anal. Chem.* **2009**, *81*, 9493−9498.
(50) *Hydrogen Cyanide and Cyanides: Human Health Aspects*. World Health Organization: Geneva, Switzerland, 2004.
(51) Kumari, N.; Jha, S.; Bhattacharya, S. An Efficient Probe for Rapid Detection of Cyanide in Water at Parts Per Billion Levels and Naked-Eye Detection of Endogenous Cyanide. *Chem. - Asian J.* **2014**, *9*, 830−837.
(52) Padmaja, G. Cyanide Detoxification in Cassava for Food and Feed Uses. *Crit. Rev. Food Sci. Nutr.* **1995**, *35*, 299−339.

DOI: 10.1021/acsami.5b06352
ACS Appl. Mater. Interfaces 2015, 7, 19509−19515